

Calibration and Validation of the InfraRed Atmospheric Sounder Onboard the FY3B Satellite

Chengli Qi, Yong Chen, Hui Liu, Chunqiang Wu, and Dekui Yin

Abstract—InfraRed Atmospheric Sounder (IRAS) instruments were successfully launched onboard the FengYun-3A (FY3A) and FengYun-3B (FY3B) satellites on May 27, 2008, and November 5, 2010, respectively. They aim at providing multichannel radiances within the spectral range of visible to infrared (IR) wavelengths for many environmental applications, including data assimilation and retrievals of global atmospheric temperature and humidity profiles. However, the velocity of the filter wheel of the first IRAS onboard FY3A is unstable and, therefore, induced a discontinuity in the measurement. The IRAS onboard FY3B works well in normal and stable operational mode since its launch without any anomaly. A variety of postlaunch calibration/validation tasks are conducted using on-orbit data during a period of three months. This paper presents on-orbit verification of IRAS instrument performance, including long-term trends of the space and warm calibration counts and noise equivalent delta radiance. The Earth scenes observed simultaneously by IRAS and Meteorological Operational Satellite Programme (METOP)/Infrared Atmospheric Sounding Interferometer were obtained and compared to demonstrate a close similarity between the two measurements. Furthermore, the IR channel observations from FY3B/IRAS are compared with those from National Oceanic and Atmospheric Administration-19/High Resolution Infrared Radiation Sounder (HIRS) equivalent channels and simulations from a radiative transfer model. The results show that some of IRAS IR channels perform very well, particularly for channels 1–10, 15, 19, and 20, compared to those of HIRS. Several channels, such as 13, 16, and 18, however, display some large biases. The causes of these increased biases are still under investigation.

Index Terms—Calibration validation, FengYun 3, InfraRed Atmospheric Sounder (IRAS), on-orbit calibration.

Manuscript received November 15, 2011; revised March 5, 2012; accepted May 3, 2012. Date of publication August 17, 2012; date of current version November 22, 2012. This work was supported in part by the Chinese Ministry of Science and Technology under 973 Project 2010CB951600, part by the Chinese National Natural Science Foundation under Project 40905014, and in part by the International Science and Technology Cooperation Program of China (2010DFA21140).

C. Qi, H. Liu, and C. Wu are with the National Satellite Meteorological Center, China Meteorological Administration, Beijing 100081, China (e-mail: qicl@cma.gov.cn; liuhui@cma.gov.cn; wucq@cma.gov.cn).

Y. Chen is with the Cooperative Institute for Research in the Atmosphere, Colorado State University, Fort Collins, CO 80523-1375 USA, and also with the Center for Satellite Applications and Research, National Environmental Satellite, Data, and Information Service, and the Joint Center for Satellite Data Assimilation, National Oceanic and Atmospheric Administration, Camp Springs, MD 20746, USA (e-mail: Yong.Chen@noaa.gov).

D. Yin is with the Shanghai Institute of Technical Physics, Chinese Academy of Sciences, Shanghai 200083, China (e-mail: yin@mail.sitp.ac.cn).

Color versions of one or more of the figures in this paper are available online at <http://ieeexplore.ieee.org>.

Digital Object Identifier 10.1109/TGRS.2012.2204268

I. INTRODUCTION

THE FengYun-3 (FY3) meteorological satellite series is the second generation of polar-orbit meteorological satellites in China. There are 11 instruments onboard with ten being new for the first time in space. The InfraRed Atmospheric Sounder (IRAS) is one of the primary instruments that observe the Earth's weather and the environment, and it provides multichannel radiances from visible (VIS) to infrared (IR) wavelengths for many applications, including radiance assimilation and retrievals of global atmospheric temperature profiles, humidity profiles, ozone content, and cloud parameters.

The spectral channel and instrument configuration of IRAS are designed similar to those of the High Resolution Infrared Radiation Sounder (HIRS) instrument onboard the National Oceanic and Atmospheric Administration (NOAA) and METOP satellites. IRAS has 26 channels, including 20 IR channels (3.7–15 μm) and six VIS and near-IR channels (0.69–1.64 μm), whereas HIRS has 20 channels (19 IR channels and one VIS channel). Fig. 1 shows the spectral response functions (SRFs) of 20 thermal infrared channels of IRAS. There is one internal warm blackbody for calibration with four platinum resistance thermometer (PRT) sensors. Each sensor has one sample in a processing package, and there are four packages for one scan line in IRAS raw data. IRAS is a discrete-stepping line-scan instrument designed to measure scene radiance in 26 spectral bands to permit the calculation of the vertical temperature and water vapor profile from the Earth's surface to about 40 km. Table I lists the instrument characteristics of IRAS. Multispectral data are obtained from a single telescope and a rotating filter wheel containing 26 individual filters [1]. An elliptical scan mirror provides cross-track scanning of 56 increments of 1.8°. The mirror steps rapidly (< 35 ms) and then holds at each position while the 26 filter segments are sampled. This action takes place each 100 ms. The instantaneous fields of view (FOVs) for each channel are approximately 1.4° in the VIS and near IR and 1.3° in the IR band which, from an altitude of 836 km, encompass areas of 20.3 and 18.9 km in diameter, respectively, at nadir on the Earth.

Table II lists the IRAS channel characteristics (the NOAA-19/HIRS corresponding channels are also listed). Channels 1–7 and 14–18, which are located at the CO₂ and N₂O absorbing bands, are used for temperature sounding from the surface to about 40-km height. Channels 11–13 were designed within the water vapor absorbing region for retrieval of water vapor profiles. Channels 8–9 and 19–20, which have weighting functions peaked near the surface, are primarily used to aid

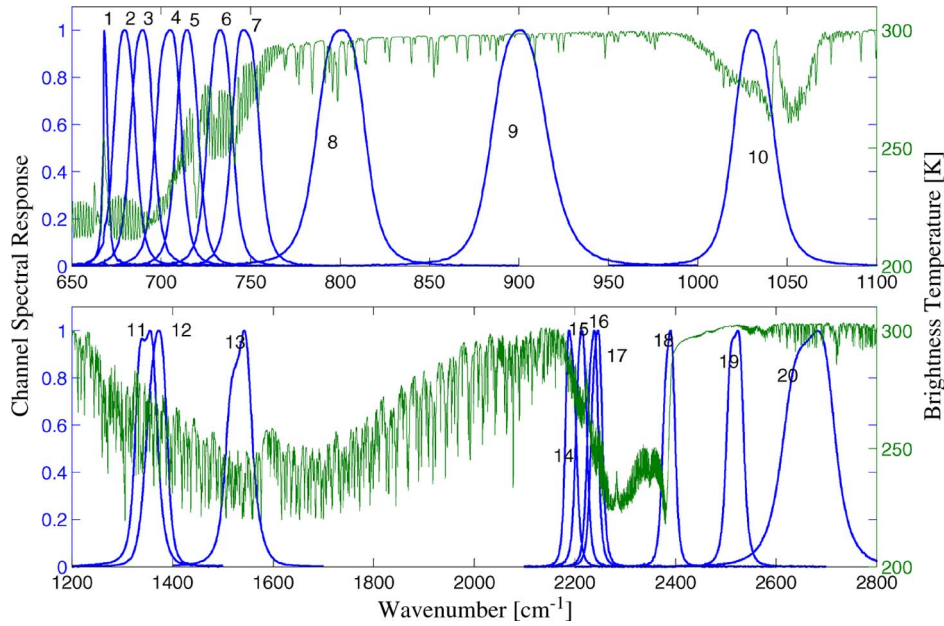


Fig. 1. FY3B/IRAS SRF for 20 IR channels.

TABLE I
FY3B/IRAS INSTRUMENT CHARACTERISTICS

Characteristic	Value
Optical Field of View	1.4 degrees VIS/NIR IR 1.3 degrees LW IR
Channel to channel registration	5%
Earth Scan Angle	49.5 degrees from nadir
Earth Scan Steps	56
Step and Dwell Time	100 msec
Total Scan plus Retrace Time	6.4 seconds
Earth Swath coverage	1127 km
Earth Field Cover	20.3 km (1.4 degrees IFOV) at nadir 18.9 km (1.3 degrees IFOV) at nadir
Radiometric Calibration	290 K IWT Blackbody and Space Look
Calibration Accuracy	1K (IR channels) 7% Albedo (ch21-24) 8% Albedo (ch25-26)
IR Detectors Temperature	100K
Signal Quantizing Levels	13 bit coding
Filter Housing Temperature	290K (normal mode) and 298K

retrieval of temperature profile by correcting the effects from surface emissivity and cloud. Channels 21–26 are mainly used for providing information of cloud and water vapor.

Calibration of the IRAS IR channels is provided by programmed views of two radiometric targets: a warm target mounted to the instrument base and a cool target view of space. Data from these two views provide sensitivity calibrations for each channel every 40 lines (256 s), if commanded. Each channel is characterized by a noise equivalent delta radiance (NE Δ N) and a set of calibration data that may be used to derive atmospheric temperatures and associated errors in the retrieval.

II. POSTLAUNCH INSTRUMENT PERFORMANCE TEST AND MONITORING

On-orbit test is a systematic and significant method for assessing the performance of satellites and instruments. After

TABLE II
FY3B/IRAS CHANNEL CHARACTERISTICS

Channel (HIRS channel)	Central Wavenumber (cm ⁻¹)	Central Wavelength (μ m)	Half Power Bandwidth (cm ⁻¹)	Absorbing Gas	NE Δ N (mW/m ² .sr.cm ⁻¹)	Energy Peak Altitude (hPa)
1 (1)	669	14.95	3	CO ₂	4.00	30
2 (2)	680	14.71	10	CO ₂	0.80	60
3 (3)	690	14.49	12	CO ₂	0.60	100
4 (4)	703	14.22	16	CO ₂	0.35	400
5 (5)	716	13.97	16	CO ₂	0.32	600
6 (6)	733	13.84	16	CO ₂ /H ₂ O	0.36	800
7 (7)	749	13.35	16	CO ₂ /H ₂ O	0.30	900
8 (10)	802	12.47	30	Window	0.20	Surface
9 (8)	900	11.11	35	Window	0.15	Surface
10 (9)	1030	9.71	25	O ₃	0.20	25
11	1345	7.43	50	H ₂ O	0.23	800
12 (11)	1365	7.33	40	H ₂ O	0.30	700
13 (12)	1533	6.52	55	H ₂ O	0.30	500
14 (13)	2188	4.57	23	N ₂ O	0.009	1000
15 (14)	2210	4.52	23	N ₂ O	0.007	950
16 (15)	2235	4.47	23	CO ₂ /N ₂ O	0.007	700
17 (16)	2245	4.45	23	CO ₂ /N ₂ O	0.007	400
18 (17)	2388	4.19	25	CO ₂	0.007	700
19 (18)	2515	3.98	35	Window	0.007	Surface
20 (19)	2660	3.76	100	Window	0.003	Surface
21(20)	14500	0.69	1000	Window	0.10%A	Cloud
22	11299	0.885	385	Window	0.10%A	Surface
23	10638	0.94	550	H ₂ O	0.10%A	Surface
24	10638	0.94	200	H ₂ O	0.10%A	Surface
25	8065	1.24	650	H ₂ O	0.10%A	Surface
26	6098	1.64	450	H ₂ O	0.10%A	Surface

the successful launch of the FengYun-3B (FY3B) satellite, VIS channels of IRAS (channels 21–26) were powered on first. About 30 days after launch, the IR channels were powered on, and the instrument was in a normal and stable status. The FY3B postlaunch on-orbit test was conducted, and the test results were checked against either the preset values in the test plans or the IRAS specifications.

One of the most significant performance parameters is the instrument sensitivity parameter NE Δ N. The prelaunch NE Δ N values were derived based on the ground vacuum calibration

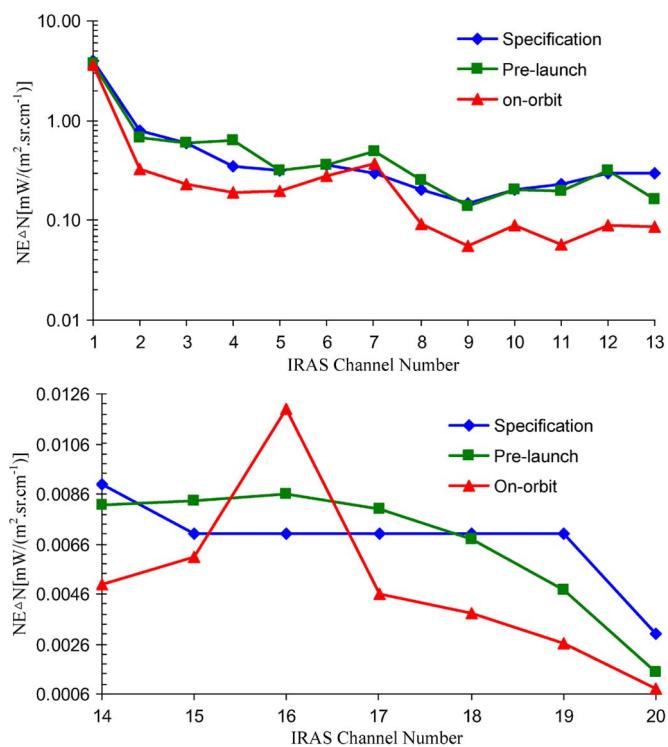


Fig. 2. NE Δ N values derived from prelaunch and on-orbit data from FY3B/IRAS.

test data. In the vacuum calibration test, the observed target was a standard source blackbody whose physical temperature can be precisely controlled, and the final NE Δ N values were determined when the standard source blackbody was at 290 K. On-orbit NE Δ N is defined as the variance in a scene radiance and is derived from the blackbody (nominally 290 K) standard deviation (STDV) noise counts multiplied by the on-orbit calibration slope. The noise counts are the STDV of the 45 measurements of blackbody, and the final NE Δ N was the average of all NE Δ N values derived from all blackbody scan lines in an orbit. The NE Δ N values calculated from prelaunch and on-orbit data are shown in Fig. 2, and it can be seen that postlaunch NE Δ N values are less than the prelaunch ones for most channels and on-orbit NE Δ N values meet the specifications except channels 7 and 16. Channel 7 has a noise slightly larger than the specification, while the noise in channel 16 is well above the prelaunch one and specification. Fig. 3 shows the channel-16 brightness temperature (BT) converted from the raw digital counts. The scattering distributed noise shown in the upper panel of Fig. 3 was found in both Earth and calibration views after launch. A 3 \times 3 pixel average-filter method was applied to pixels whose BT difference from the average measurement of a 3 \times 3 pixel window was larger than 5 K, and the filtered data are shown in the lower panel of Fig. 3. After the filtering process, the NE Δ N of channel 16 was halved and meets the specification.

The FY3 instrument performance monitoring platform for IRAS has been established since the FengYun-3A (FY3A) satellite was launched; the monitoring parameters include calibration coefficients, blackbody and space view counts, and

instrument noise (NE Δ N). The system also monitors the instrument status parameters, including component temperature and voltage information.

Time series of FY3B/IRAS warm calibration counts (internal warm-blackbody target count), cold calibration counts, channel gains, and noise are shown in Figs. 4–7, respectively. It is clearly shown that, in the early months, both the cold and warm calibration counts presented a fast variation status and, then, the variation trend became a little flat in the latest months. The first ten channels experience relatively more attenuated counts for space views than for blackbody views, so the slope calibration coefficients show a little rise trend. As for cold space view counts, channels 8 and 10 have the largest magnitude of attenuation; the attenuated count reached 400 for channel 8 and 300 for channel 10, which are the same as those of FY3A IRAS, while the attenuated count of blackbody is about 20, so these two channels demonstrate a relatively sharp decay curve. Noise has a relatively stable status except in the end of August: There is a sharp jump for channels 4, 7, and 17.

III. CALIBRATION ALGORITHM FOR FY3/IRAS

There are two working models for IRAS when it is in normal operational status: calibration mode and scanning mode. They operate alternately in an observation cycle of 40 scan lines. In the former mode, the scan mirror points to the calibration objects of cold space and onboard blackbody so it involves two scan lines, while in the latter mode, the scan mirror points to Earth scene and it includes 38 scan lines. For scanning mode, all the 56 measurements are effective, but for calibration-mode scan lines, only the former 45 measurements are effective and the residual 11 data fields are electronic correction information.

The variable that describes the magnitude of the radiance that the instrument observes is digital counts in raw L0 data set, but the commonly used variable in satellite data application is radiance. Radiance calibration is the process of deriving the transfer function between digital counts and the scene channel radiances. There are two individual calibration processes in the lifetime of an instrument: prelaunch calibration and on-orbit calibration. Prelaunch calibration was conducted through ground vacuum IR calibration test before the satellite’s launch, and the function of transferring digital counts to radiance has been established through the quadratic

$$r = a_0 + a_1 C_v + a_2 C_v^2 \tag{1}$$

where C_v is the counts from the view, r is the corresponding radiance, and a_0 , a_1 , and a_2 are the calibration coefficients; a_1 is the slope which directly shows the response of counts to the input radiance signals and can be used to monitor the response rate of the detector of an instrument as an important parameter. In a vacuum IR calibration test, the instrument viewed an outside standard source blackbody whose temperature was controlled precisely and was set at intervals of 10° in the range of 200–280 K and 5° in the range of 285–340 K (overall, 21 temperature levels). Radiance that the instrument’s detector received can be calculated from the transfer function of the

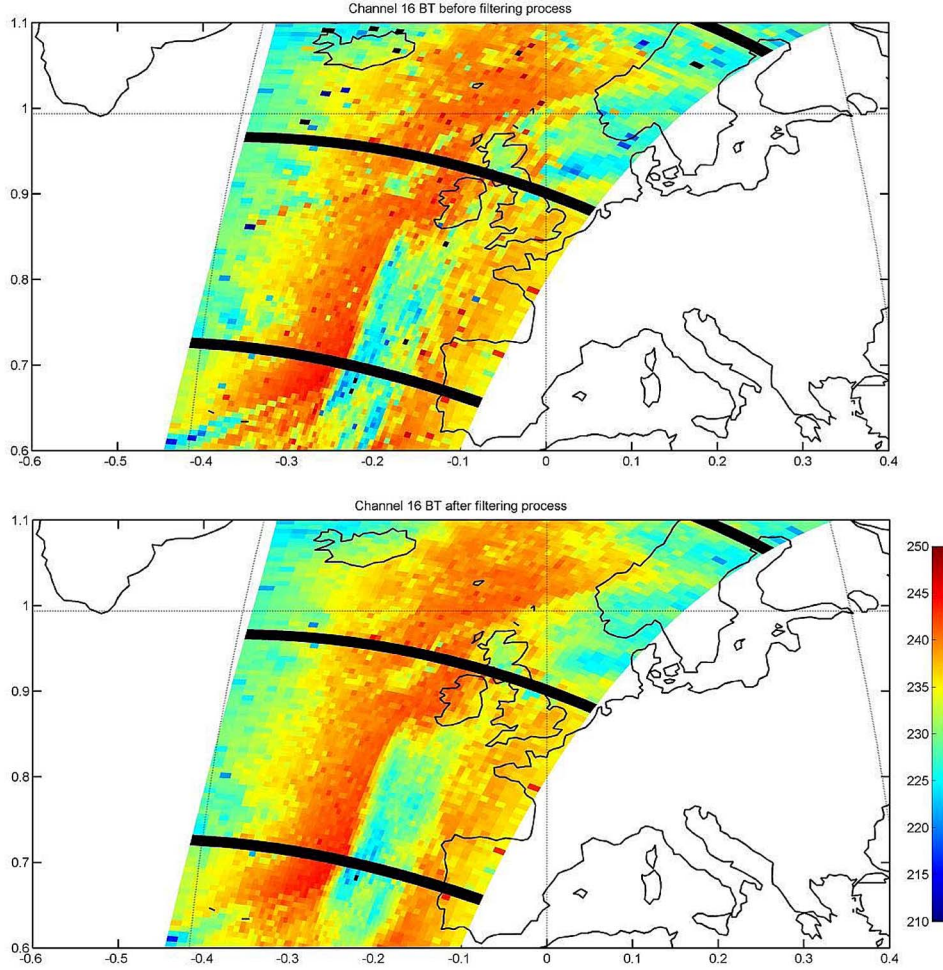


Fig. 3. Channel-16 BT before and after filtering process.

standard blackbody from the 21 groups of radiance and counts, and the calibration coefficients are derived from these groups.

When the satellite was launched, the instrument was in an on-orbit environment which was different from the ground vacuum test (an approximate vacuum condition). Therefore, the calibration coefficients obtained from prelaunch calibration were no longer applicable and need to establish a new calibration relation using on-orbit environment data. While the onboard data that can be used for calibration were only observations of space view and internal blackbody view whose radiance can be estimated and can only get the coefficients of a_0 and a_1 , a_2 maintained the value that was computed from the ground calibration process and will not change throughout the lifetime of the instrument (see Table III). The detail of the calibration process is similar to that of HIRS (see NOAA KLM User’s Guide: <http://www.ncdc.noaa.gov/oa/pod-guide/ncdc/docs/klm/html/c7/sec7-2.htm>). The on-orbit coefficients a_0 and a_1 in (1) can be determined by applying it to the views of space and the internal target

$$0 = a_0 + a_1 C_s + a_2 C_s^2 \tag{2}$$

$$r_b = a_0 + a_1 C_b + a_2 C_b^2 \tag{3}$$

where C_s and C_b are the mean counts from the 45 views of space and the internal target, respectively. Radiance from the space is assumed to be zero, and r_b is the radiance of the internal target. The counts for the space and internal target views are each averaged over the range of the 45 measurements, and the unsatisfactory conditions are thrown out by using a 3σ (STDV) criterion. The count from the internal target PRT views is transformed to temperatures by a quartic relation. For each IR channel (1–20), the blackbody radiance r can be computed from the Planck relation

$$r = \frac{c_1 v^3}{\left[\exp\left(\frac{c_2 v}{T^*}\right) - 1 \right]} \tag{4}$$

where c_1 and c_2 are the Planck function constants, ν is the central wavenumber, computed prior to the launch of the satellite and based on the channel SRF $\phi(\nu)$

$$\nu = \frac{\int \phi(\nu) \nu d\nu}{\int \phi(\nu) d\nu} \tag{5}$$

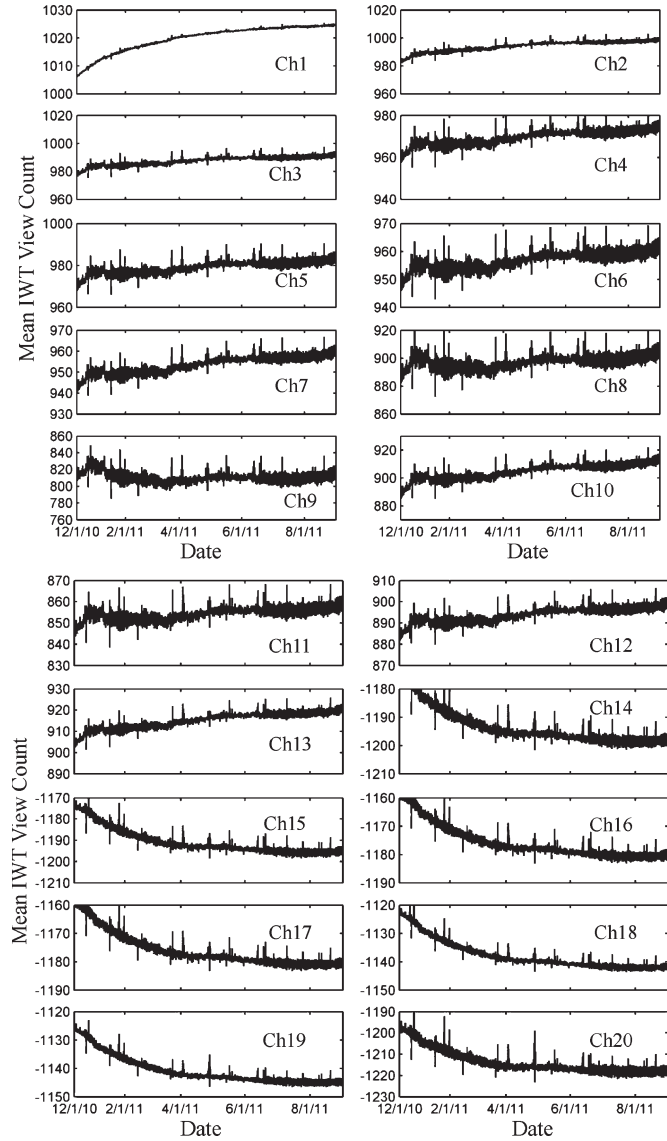


Fig. 4. Long-term trends of onboard warm-blackbody calibration counts as a function of date since launch for FY3B/IRAS.

and T^* is the channel effective BT at the central wavenumber ν , defined by

$$T^* = b + cT \quad (6)$$

where b and c are the channel-dependent band-correction coefficients [2] computed based on a group of simulations of temperature and effective BT before the launch of the satellite and T is the blackbody temperature of the internal target PRT. The slope intercepts a_1 and a_0 then become

$$a_1 = \frac{r_b - a_2(C_b^2 - C_s^2)}{C_b - C_s} \quad (7)$$

$$a_0 = -a_2 C_s^2 - a_1 C_s. \quad (8)$$

The IRAS instrument detector receives all radiation that falls on it. The instrument temperature is carefully controlled to minimize false fluctuations from other components, so that most optical components experienced slowly changed tem-

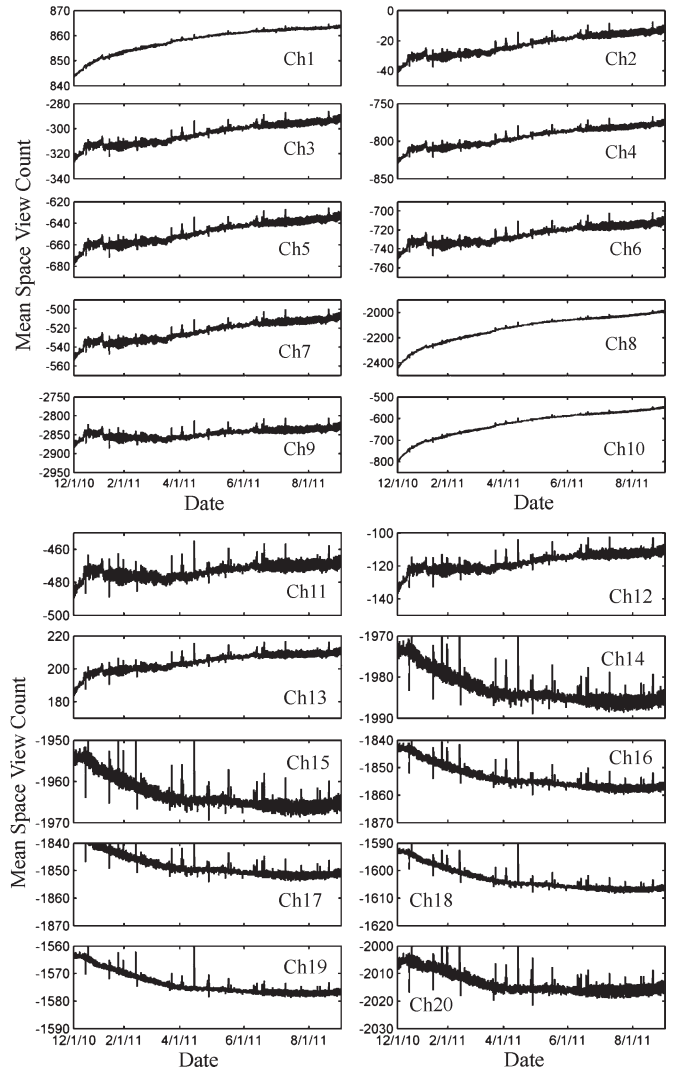


Fig. 5. Long-term trends of cold space calibration counts as a function of date since launch for FY3B/IRAS.

perature between calibration cycles (every 40 scan lines or 256 s). Calibration coefficients on calibration observation scan line (scan line of inner blackbody and space) were computed according to the aforementioned steps and then interpolated to the 38 Earth view scan lines between two calibration cycles. When coefficients are applied to Earth view counts, one can calculate the corresponding radiance and BT and accomplish the calibration process.

IV. VALIDATION OF IRAS OBSERVATION

A. Intersatellite Validation of Observation

Validation of IRAS measurements was conducted by two methods. The first one is an intersatellite comparison using hyperspectral instrument on a low Earth orbiting satellite, such as the Atmospheric Infrared Sounder (AIRS) and the Infrared Atmospheric Sounding Interferometer (IASI). AIRS and IASI have been chosen as standard because they are versatile to be collocated in space and converted in spectrum to compare with any broadband IR sensors. It has also been validated that

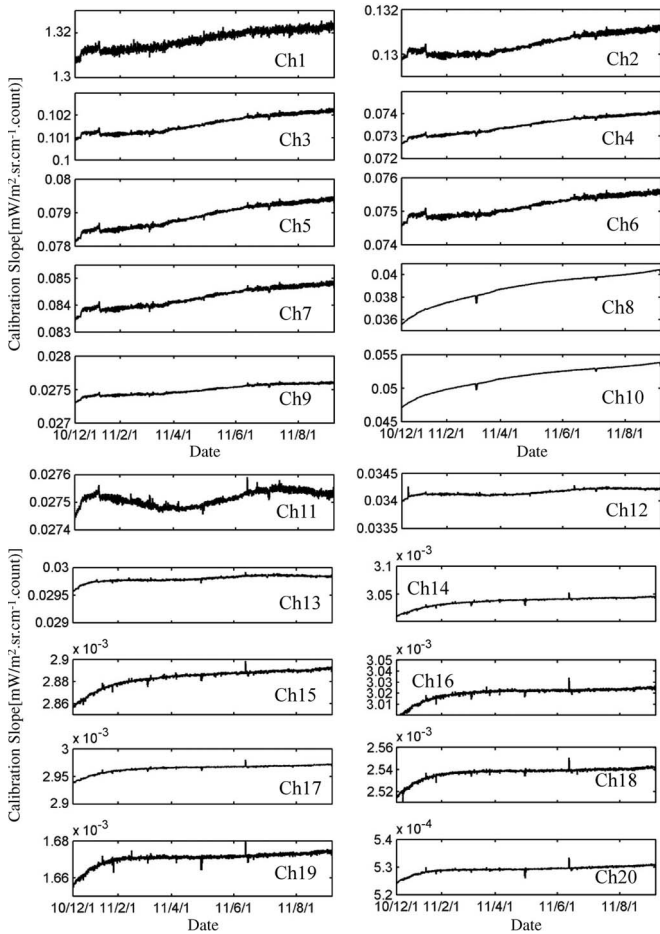


Fig. 6. Long-term trends of channel calibration coefficients (slope) since the launch for FY3B/IRAS.

TABLE III
FY3B/IRAS QUADRATIC CALIBRATION COEFFICIENTS

Channel	a_2 ($mW/(m^2 \cdot sr \cdot cm^{-1} \cdot count^2)$)	Channel	a_2 ($mW/(m^2 \cdot sr \cdot cm^{-1} \cdot count^2)$)
1	-2.63E-04	11	2.79E-08
2	-5.27E-07	12	5.42E-08
3	-1.00E-07	13	3.19E-07
4	7.88E-08	14	-3.72E-09
5	9.10E-08	15	-2.68E-09
6	-2.43E-07	16	-4.30E-09
7	-9.68E-08	17	-3.20E-09
8	3.59E-08	18	-2.64E-09
9	1.39E-08	19	-2.13E-09
10	4.10E-08	20	6.23E-11

AIRS and IASI measurements are highly accurate [3], [4] and consistent with each other [5]–[9].

IASI was chosen as a reference standard in validation of IRAS. Intersatellite radiance bias between the IRAS on FY3B

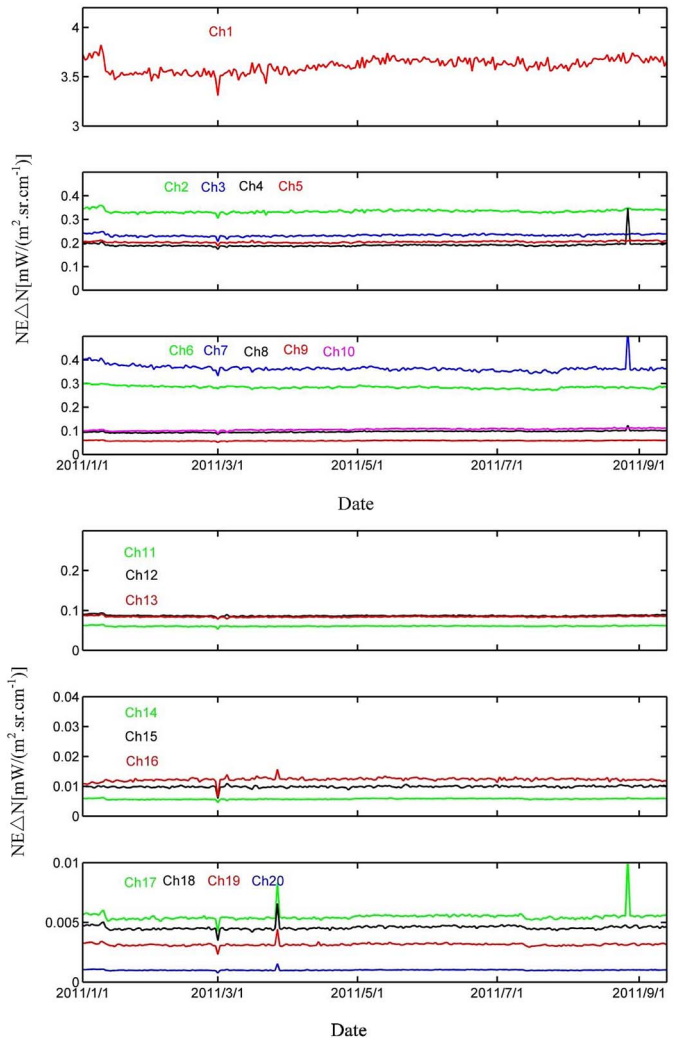


Fig. 7. Long-term trends of NEΔN as a function of date since launch for FY3B/IRAS.

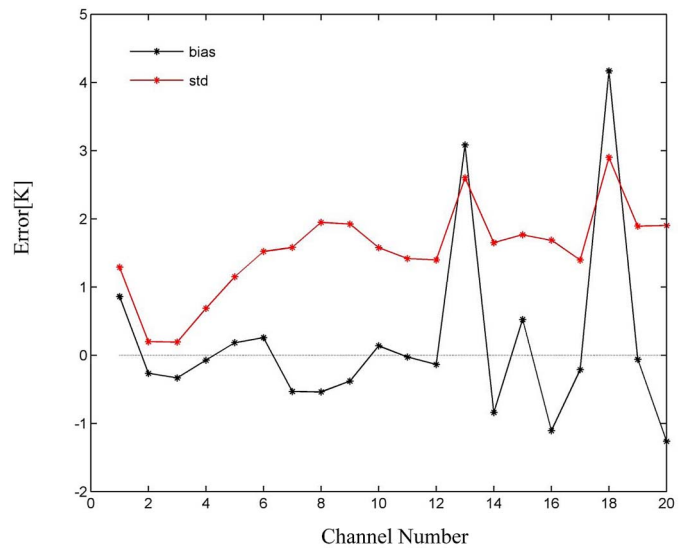


Fig. 8. Bias characteristics from SNO between IRAS and IASI.

and IASI on METOP is identified by comparing the radiance measurements of the simultaneous nadir overpass (SNO) at the orbital intersections of two satellites, which occurred mostly in

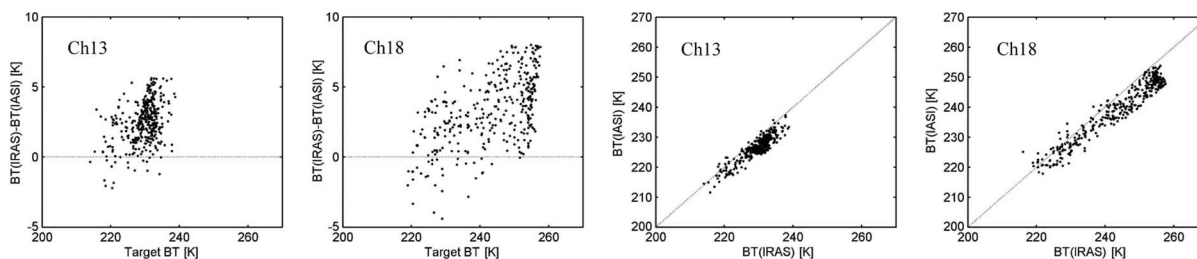


Fig. 9. Bias characteristics with target BT and BT of IRAS versus that of IASI.

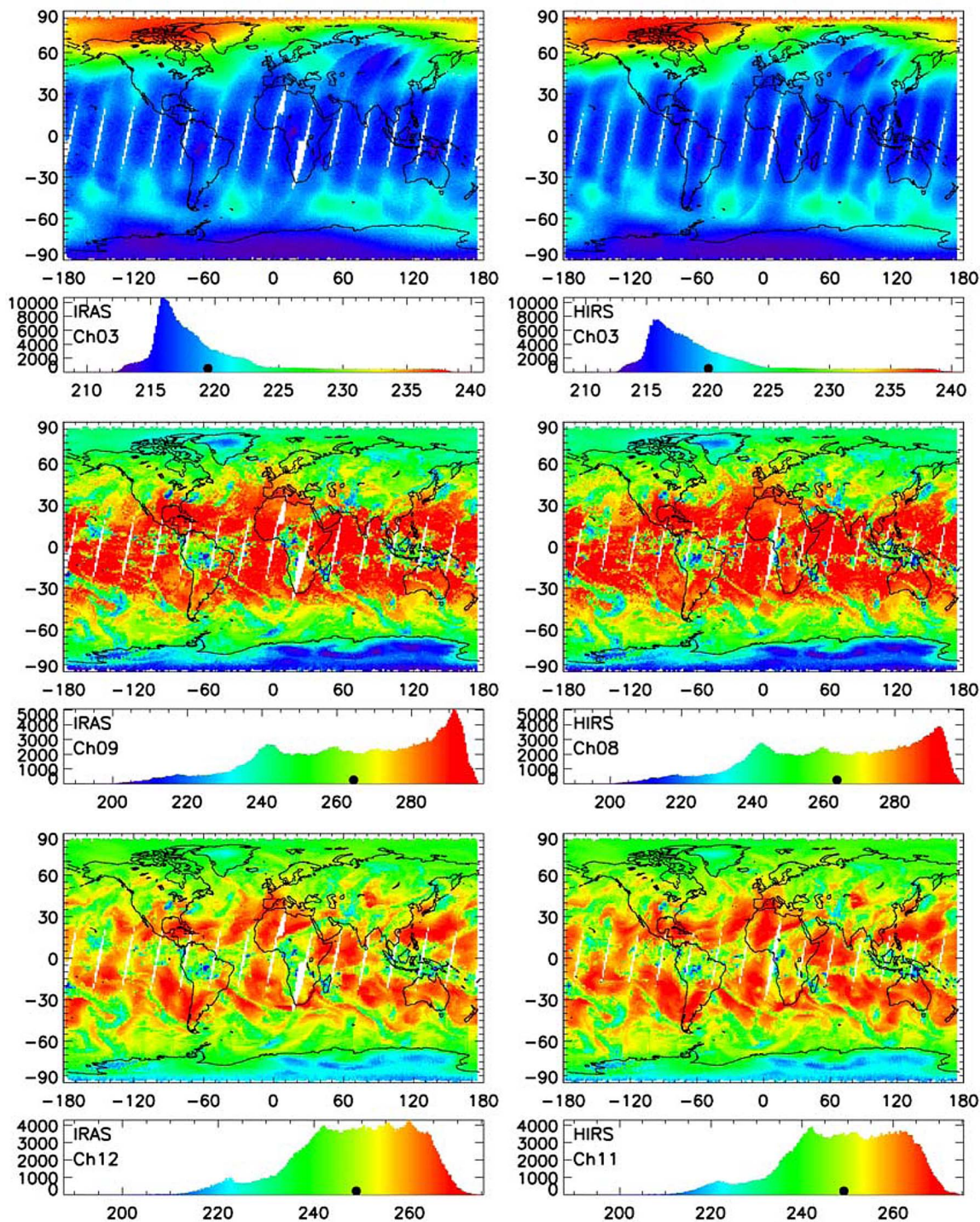


Fig. 10. Observed BTs for (left column) FY3B/IRAS and (right column) the equivalent NOAA-19/HIRS channels. For each channel (channels 3, 9, and 12), top panel shows the global distribution, and bottom panel shows the histogram (for the descendent orbits on April 9, 2011). The spot at the base of the histograms indicates the mean BT for each plot.

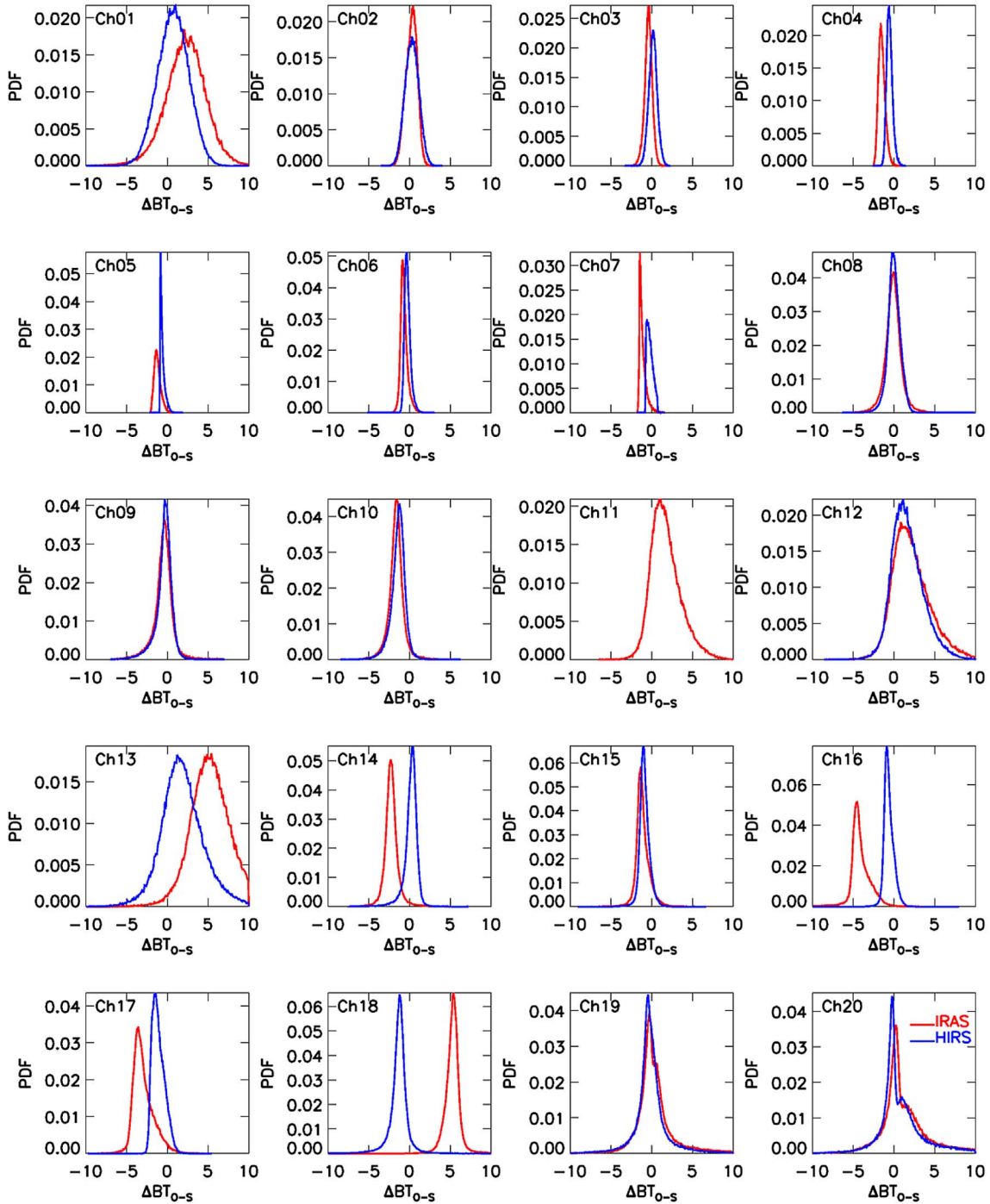


Fig. 11. PDFs of bias between observations and CRTM simulations for (red) IRAS and (blue) HIRS under clear sky and over ocean from April 9 to April 15, 2011.

polar regions every several days. Since the SNO observations are taken at nearly the same time, at the same location, and at nadir, this eliminates the effects of satellite observation time and view angle differences. SNO methods have been extensively applied in postlaunch calibration in order to quantify intersatellite observation biases objectively and accurately [10].

Six-month data of IRAS and IASI from January 2011 to June 2011 were collected for the intersatellite validation. Pixels at the SNO are identified if the ground distance is less than

10 km and the time difference is less than 10 min. Spatial subsets are extracted for 5×5 IASI pixels and 3×3 IRAS pixels of which the central ones meet the aforementioned conditions. IASI is a Michelson interferometer that measures IR radiation in the spectral region of from 3.6 to $15.5 \mu\text{m}$ with a spectral resolution of 0.5 cm^{-1} and a spectral sampling interval of 0.25 cm^{-1} . However, IRAS IR channels have very broad SRFs; we cannot directly compare the radiances from IASI with those from IRAS. Therefore, we first use measured IASI spectra to

convolve the IRAS SRFs and get the IASI convolved IRAS channel radiances

$$R_{COV} = \frac{\int R_{IASI}(\nu)\phi(\nu)d\nu}{\int \phi(\nu)d\nu} \quad (9)$$

where R_{COV} is the convolved IRAS channel radiance and $R_{IASI}(\nu)$ is the IASI channel radiance. Then, R_{COV} is compared to the IRAS measurement.

A quality control in (10) is also made for the 5×5 IASI pixels after convolution to remove these high inhomogeneous observations

$$\frac{STDV_{IASI}}{MEAN_{IASI}} < 0.1. \quad (10)$$

If the statistical parameter of the 5×5 IASI pixels meets (10), the mean value of them was chosen and compared with the corresponding mean value of the 3×3 IRAS pixels. Statistical comparisons are performed by calculating the mean and STDV of the BT difference between IRAS and IASI. Fig. 8 shows the comparison results between IRAS and IASI. The mean bias for most channels is less than 1 K. Channels 13 and 18 exhibit the largest positive bias of 3–4 K. The BT difference versus scene temperature is shown in Fig. 9, and it shows that more positive bias occurs in higher scene BT range; this indicates that nonlinearity still exists apparently. It can also be seen that the standard error tends to be larger for channels with weighting functions that peak lower in the atmosphere (see Table II); this is probably because the channels that detect atmosphere of near boundary layer were more susceptible to the time and location differences even though they are carefully controlled in SNO method.

B. Theoretical Simulation and Observation of BT

The second method to evaluate satellite observation is comparison between measurements and model simulation. In this paper, we used the Community Radiative Transfer Model (CRTM) to simulate IRAS channel BTs. CRTM is a sensor-based fast radiative transfer model developed at the Joint Center for Satellite Data Assimilation [11]–[14]. It can be used to simulate both radiances at the top of atmospheres and radiance gradients (or Jacobians) for satellites over various atmospheric and surface conditions and is a key component in the data assimilation system of numerical weather prediction models.

Due to the difficulties of specifying surface emissivity over land and relatively lower accuracy of model simulation in cloudy or rainy conditions (except for microwave observation), we only simulated the clear sky BT over ocean. For better comparisons between similar sensors, NOAA-19/HIRS measurements were also simulated and compared through the same method.

The atmospheric profiles and surface fields from the 6-h forecast fields of the National Centers for Environmental Prediction (NCEP) Global Forecast System (GFS) were used as inputs to CRTM. However, over ocean, the GFS sea surface temperatures were replaced by Operational Sea Surface Temperature and Sea

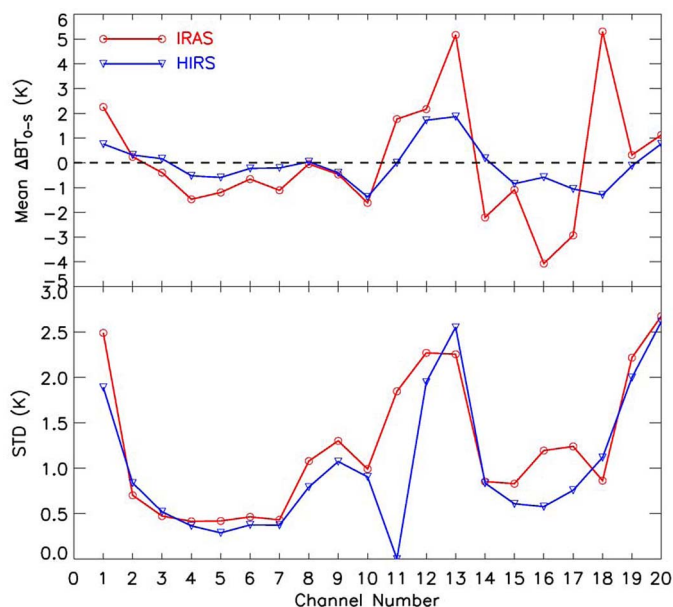


Fig. 12. Mean bias and STDV of observations compared with CRTM simulations for (red) IRAS and (blue) HIRS under clear sky and over ocean from April 9 to April 15, 2011.

Ice Analysis (OSTIA) system global sea surface temperature. The OSTIA data are daily global-coverage $1/20^\circ$ (~ 6 km) high-resolution data set from the U.K. Met Office [15]. The GFS atmospheric profiles (pressure, temperature, water vapor, and ozone) had 65 vertical levels on a global grid of 0.3125° spatial resolution. For a given satellite pixel, the spatial and temporal interpolation from the forecast fields is performed as follows: First, the four analysis grid points surrounding the satellite pixel were bilinearly interpolated to the location of satellite pixel location, and then, a linear temporal interpolation in time was performed using two forecast fields that bound the IRAS (and HIRS) observational time.

In this paper, one-week observation data from April 9 to April 15, 2011, were selected for comparison with CRTM model simulations for FY3B/IRAS and NOAA-19/HIRS. Both FY3B and NOAA-19 satellites are afternoon satellites with local time of ascending node at 13:30 P.M. and 13:31 P.M., respectively; therefore, IRAS and HIRS have very similar temporal and spatial coverage. As an example, Fig. 10 shows the observed BTs for IRAS and the equivalent HIRS channels. For each channel (IRAS channels 3, 9, and 12, corresponding to HIRS channels 3, 8, and 11), the results are shown for the global distribution and histogram for the descending orbits on April 9, 2011. From an inspection of the histograms of BTs, it is evident that IRAS BTs, at the peaks in the histograms, are just slightly shifted (less than 1 K) relative to the HIRS observations for the three channels.

The comparison between observations and CRTM simulations was performed only over ocean between the $\pm 65^\circ$ latitude zone and in clear sky conditions. To detect cloud pixel, a very simple method is used as follows based on [16]: The three CO_2 channels 4, 5, and 7 (at 14.22, 13.97, and $13.35 \mu\text{m}$) are used to detect the presence of high clouds if, for a FOV, the expected clear (from CRTM simulation) minus measured

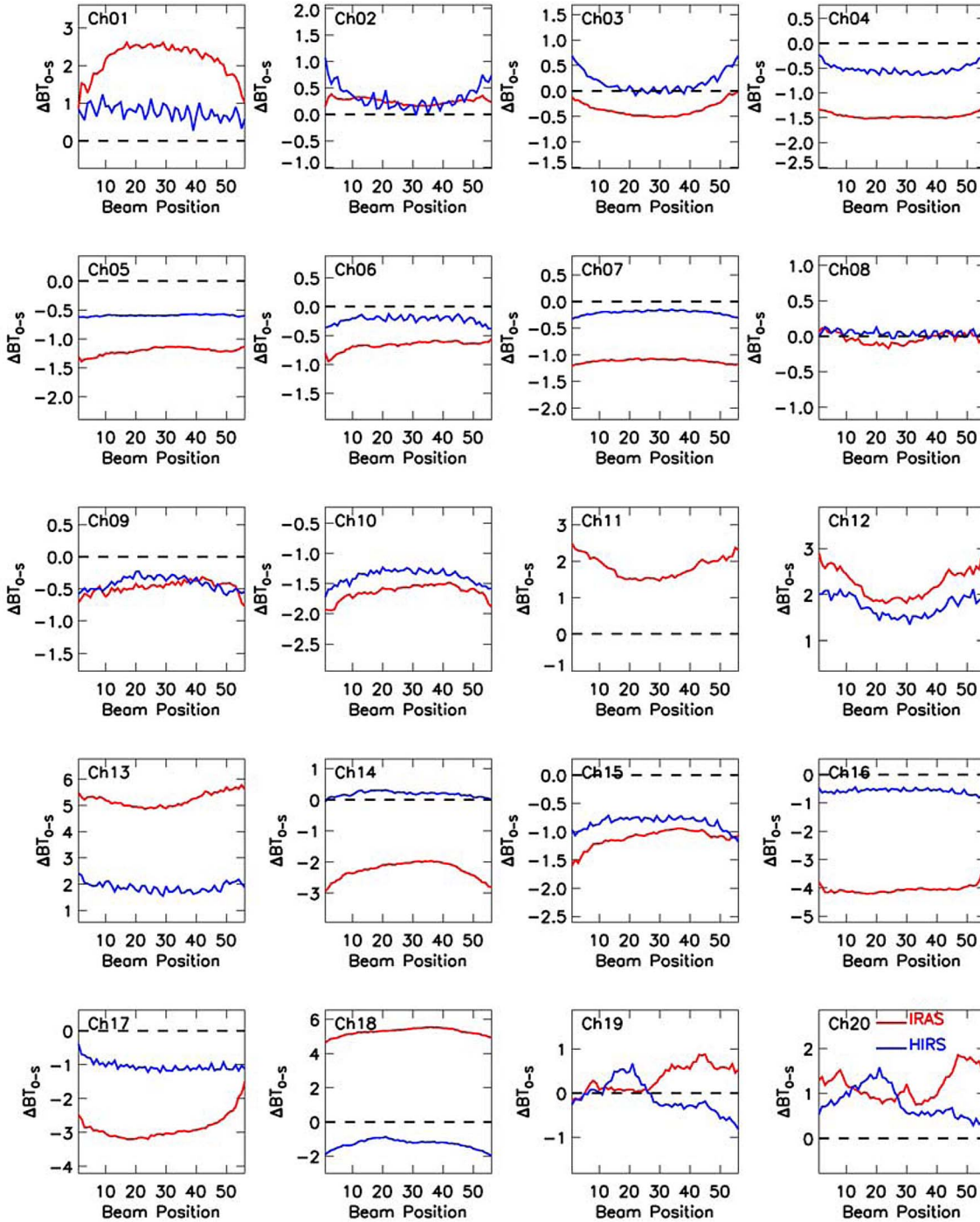


Fig. 13. Scan angle biases as a function of beam position of observations compared with CRTM simulations for (red) IRAS and (blue) HIRS under clear sky and over ocean from April 9 to April 15, 2011.

radiance ($R_{clr} - R_m$) is greater than five times of the instrument noise level ($R_{clr} - R_m > 5 \text{ NE}\Delta N$). In addition, the window channel of $11.11 \mu\text{m}$ (IRAS channel 9 and HIRS channel 8) is used to detect the low cloud if the moisture correction BT is 2.5 K above the sea surface temperature.

Fig. 11 shows the probability distribution function (PDF) of bias between observations and CRTM simulations for IRAS and HIRS over ocean under clear sky from April 9 to April 15, 2011. The bias distributions of IRAS are quite consistent with those of HIRS at most channels,

particularly for CO_2 sounding channels. Larger differences exist in channels 13, 14, and 16–18. The mean bias and STDV between observations and simulations for IRAS and HIRS are shown in Fig. 12 (note that there is no HIRS equivalent channel to IRAS channel 11 and the mean and STDV for this channel in HIRS are set to zero). The maximum bias between observation and simulation for IRAS is about 5 K at channels 13 and 18, and the minimum is less than 0.05 K at channel 8. For HIRS, the maximum bias (1.9 K at channel 13) is smaller than that of IRAS, and the minimum bias

(0.04 K at channel 8) is similar to that of IRAS. Overall, HIRS shows better and more consistent performance than IRAS. Some IRAS channels exhibit unexpected relatively large biases (channels 13, 16, and 18, which is consistent with the SNO validation conclusion), which may be contributed by several sources, such as instrument calibration processing, variation of instrument spectral characteristics after test (such as SRF), instrument parameters, and background field and/or model errors, and need to be further investigated which is beyond the scope of this work. Fig. 12 also shows the STDV for IRAS and HIRS. Both the magnitude and trend of the two STDV distributions are quite consistent at all corresponding channels. Channels 3–6 exhibit the smallest STDVs, while the surface-sensitive sounding channels, such as 19 and 20, display the largest STDVs, which is consistent with the results from the intersatellite comparison. The reason for this distribution is that the impacts of surface parameters and cloud on simulation are greater for surface-sensitive channels, such as 19 and 20, while, for atmospheric sounding channels, such as channels 3 and 6, the impacts are smaller. The difference between IRAS and HIRS is small (less than 0.7 K for all channels) which indicates that the observation from IRAS may be considered to be used in NWP models, although more test should be done. We also compared the scan angle biases as a function of beam position of observations compared with CRTM simulations for IRAS (red) and HIRS (blue) over ocean under clear sky from April 9 to April 15, 2011, which is shown in Fig. 13. Most of the channels show angle-dependent bias for both IRAS and HIRS, although HIRS shows much smaller bias, which should be carefully removed in satellite data assimilation systems in order to fulfill the assumptions that the observation errors are nonbiased and that they follow Gaussian distributions.

V. SUMMARY AND CONCLUSION

On-orbit test is an absolutely necessary step for a satellite and an instrument after its launch. The IRAS operational calibration algorithms work normally and well, leading to the successful on-orbit test and instrument performance monitoring. On-orbit verification of instrument performance which includes long-term trends of the space and warm calibration counts and NE Δ N was conducted. On-orbit NE Δ N values meet specifications except channels 7 and 16. Both the cold and warm calibration counts presented a high variation status in the early months and became a little flat in the latest months. Counts from cold space view for channels 8 and 10 have the largest magnitude of attenuation, which is the same to IRAS on FY3A. Channels 8 and 10 have the sharpest decay curve of calibration slopes, which is corresponding to the decrease status of cold counts. Noise has a relatively stable status except in the end of August: a sharp jump for channels 4, 7, and 17.

Intersatellite comparisons between IRAS and METOP/IASI were performed and demonstrated a close similarity between the two measurements. Furthermore, the distributions of BTs from FY3B/IRAS and NOAA-19/HIRS are also compared with simulations from a radiative transfer model. Some larger dif-

ferences exist for some channels; further study will be needed to understand the reasons. The study results shown in this paper will provide useful information in future validation and application for this kind of IR instruments.

ACKNOWLEDGMENT

The authors thank Dr. F. Weng and Prof. X. Zou for their very useful suggestions to improve our paper.

REFERENCES

- [1] D. K. Yin, "Flight model design report of InfraRed Atmospheric Sounder onboard FY3 satellite," Shanghai Inst. Tech. Phys. Chin. Acad. Sci., Shanghai, China, 2006.
- [2] Y. Chen, F. Weng, Y. Han, and Q. Liu, "Planck weighted transmittance and correction on solar reflection for broadband infrared satellite channels," *J. Atmos. Ocean. Technol.*, vol. 29, no. 2, pp. 382–396, Mar. 2012, JTECH-D-11-00102.
- [3] D. C. Tobin, H. E. Revercomb, R. O. Knuteson, F. A. Best, W. L. Smith, N. N. Ciganovich, R. G. Dedecker, S. Dutcher, S. D. Ellington, R. K. Garcia, H. B. Howell, D. D. LaPorte, S. A. Mango, T. S. Pagano, J. K. Taylor, P. van Delst, K. H. Vinson, and M. W. Werner, "Radiometric and spectral validation of Atmospheric Infrared Sounder observations with the aircraft-based scanning high-resolution interferometer sounder," *J. Geophys. Res.*, vol. 111, no. D9, pp. D09S02-1–D09S02-14, Mar. 2006. doi:10.1029/2005JD006094.
- [4] D. Blumstein, B. Tournier, F. R. Cayla, T. Phulpin, R. Fjortoft, C. Buil, and G. Ponce, "In-flight performance of the Infrared Atmospheric Sounding Interferometer (IASI) on METOP-A," in *Proc. SPIE—Atmospheric Environmental Remote Sensing Data Processing Utilization III: Readiness GEOSS*, San Diego, CA, 2007, pp. 66840H-1–66840H-12.
- [5] H. H. Aumann and T. S. Pagano, "Using AIRS and IASI data to evaluate absolute radiometric accuracy and stability for climate applications," in *Proc. SPIE—Atmospheric Environmental Remote Sensing Data Processing Utilization IV: Readiness GEOSS II*, San Diego, CA, 2008, pp. 66840H-1–66840H-12.
- [6] D. Blumstein, E. Pequignot, B. Tournier, R. Fjortoft, L. Buffet, C. Larigauderie, T. Phulpin, and I. Gaudel, "IASI FM2 on METOP A Performances after 1.5 year in orbit," in *Proc. 16th Int. TOVS Study Conf.*, Angra dos Reis, Brazil, 2008.
- [7] L. Strow, S. Hannon, D. Tobin, and H. Revercomb, "Inter-calibration of the AIRS and IASI operational infrared sensors," in *Proc. 17th Annu. CALCON Tech. Conf.*, Logan, UT, 2008.
- [8] D. C. Tobin, H. Revercomb, F. Nagle, and R. Holz, "Evaluation of IASI and AIRS spectral radiances using simultaneous nadir overpasses," in *Proc. 16th Int. TOVS Study Conf.*, Angra dos Reis, Brazil, 2008.
- [9] L. Wang, X. Wu, Y. Li, M. Goldberg, S. H. Sohn, and C. Cao, "Comparison of AIRS and IASI radiances using GOES imagers as transfer radiometers towards climate data records," *J. Appl. Meteorol. Climatol.*, vol. 49, no. 3, pp. 478–492, Mar. 2010.
- [10] C. Cao, H. Xu, J. Sullivan, L. McMillin, P. Ciren, and Y. T. Hou, "Intersatellite radiance biases for the high-resolution infrared radiation sounders (HIRS) on board NOAA-15, -16, and -17 from simultaneous nadir observations," *J. Atmos. Ocean. Technol.*, vol. 22, no. 4, pp. 381–395, Apr. 2005.
- [11] F. Weng, Y. Han, P. van Delst, Q. Liu, and B. Yan, "JCSDA Community Radiative Transfer Model (CRTM)," in *Proc. 14th Int. ATOVS Study Conf.*, Beijing, China, 2005, pp. 217–222.
- [12] Y. Han, P. van Delst, Q. Liu, F. Weng, B. Yan, R. Treadon, and J. Derber, "Community Radiative Transfer Model (CRTM)-version 1," NOAA, Washington, DC, NOAA Tech. Rep. NESDIS 122, p. 40, Aug. 2006.
- [13] Y. Chen, F. Weng, Y. Han, and Q. Liu, "Validation of the Community Radiative Transfer Model (CRTM) by using CloudSat data," *J. Geophys. Res.*, vol. 113, no. 6, pp. D00A03-1–D00A03-15, 2008. doi:10.1029/2007JD009561.
- [14] Y. Chen, Y. Han, P. van Delst, and F. Weng, "On water vapor Jacobian in fast radiative transfer model," *J. Geophys. Res.*, vol. 115, no. 12, pp. D12303-1–D12303-20, 2010. doi:10.1029/2009JD013379.
- [15] J. D. Stark, C. J. Donlon, M. J. Martin, and M. E. McCulloch, "OSTIA: An operational, high resolution, real time, global sea surface temperature analysis system," in *Proc. IEEE OCEANS—Marine Challenges: Coastline to Deep Sea*, Aberdeen, Scotland, 2007, pp. 1–4.
- [16] D. P. Wylie and W. P. Menzel, "Eight years of high cloud statistics using HIRS," *J. Climate*, vol. 12, no. 1, pp. 170–184, 1999.



Chengli Qi was born in Hunan, China, on July 12, 1979. She received the M.S. degree in atmospheric physics from the Chinese Academy of Meteorological Sciences, Beijing, China, in 2004.

She is currently a Research Associate with the National Satellite Meteorological Center, China Meteorological Administration, Beijing, where she is also the Instrument Scientist of the InfraRed Atmospheric Sounder (IRAS) on board the FY3 satellite series. Her research activities include development and application of an operational algorithm for cali-

brating the IRAS on board FY3A/FY3B polar-orbiting satellites, development of engineering software to process IRAS L1 product, and working on infrared instrument cross-calibration and radiative transfer model simulation.



Chunqiang Wu received the B.S. degree in atmospheric science from Zhejiang University, Hangzhou, China, in 2005 and the M.S. and Ph.D. degrees in meteorology from the Institute of Atmospheric Physics, Chinese Academy of Sciences, Beijing, China, in 2007 and 2010, respectively.

Since July 2010, he has been with the National Satellite Meteorological Center, China Meteorological Administration, Beijing, where he was responsible for developing the algorithms to retrieve atmospheric parameters from the infrared sounders

aboard the FY3/4 satellite series and is currently an Assistant Scientist. His research interests include deriving atmospheric temperature and moisture profiles from the hyperspectral sounder under all weather conditions.



Yong Chen received the Ph.D. degree from the University of California, Los Angeles, in 2005.

He is currently a Research Scientist with the Cooperative Institute for Research in the Atmosphere, Colorado State University, Fort Collins. Since March 2006, he has been with the Center for Satellite Applications and Research, National Environmental Satellite, Data, and Information Service, and the Joint Center for Satellite Data Assimilation, National Oceanic and Atmospheric Administration, Camp Springs, MD, to develop and validate the Community

Radiative Transfer Model (CRTM) under various atmospheric and surface conditions. CRTM has been successfully used in several operational data assimilation systems in the U.S. He has published over 15 papers in international peer-reviewed journals. The major fields that he is working on include the development and implementation of new components into CRTM, validation of CRTM under various atmospheric and surface conditions, assimilation impacts of satellite measurements on global numerical weather prediction models, and four radiative transfer theory and applications.



Dekui Yin was born in Anhui, China, on September 15, 1964. He received the Ph.D. degree from the Northwestern Polytechnical University, Xi'an, China, in 1996.

He is currently a Researcher with the Shanghai Institute of Technical Physics, Chinese Academy of Sciences, Shanghai, China. These years, he is mainly engaged in the development of the InfraRed Atmospheric Sounder aboard the Chinese FengYun-3 meteorological satellite, and specializes in infrared technology, signal processing, instrument

calibration, etc.



Hui Liu was born in Heilongjiang, China, on October 22, 1974. She received the M.S. degree in atmospheric physics from the Chinese Academy of Meteorological Sciences, Beijing, China, in 2006.

Since 2006, she has been with the National Satellite Meteorological Center, China Meteorological Administration, Beijing. Her major is in radiation transfer theory and atmospheric remote sensing. Her current interests include atmospheric sounding with high-spectral-resolution sensors, such as Atmospheric Infrared Sounder and Infrared Atmospheric

Sounding Interferometer, The Advanced TIROS Operational Vertical Sounder's data preprocessing, and atmospheric radiation transfer calculations with Line-by-Line Radiative Transfer Model and Community Radiative Transfer Model.